X-ray diffraction study of a new phase of MgO at exo-planet interior pressures.

F. Coppari[1], R. F. Smith[1], J. H. Eggert[1], J. Wang[2], J. R. Rygg[1],
A. Lazicki[1], J. A. Hawreliak[1], G. W. Collins[1], T. S. Duffy[2]

[1] *Physics Division, Physical and Life Science Directorate,*
Lawrence Livermore National Laboratory, Livermore, CA 94550, USA

[2] *Department of Geosciences, Princeton University, Princeton, New Jersey, 08544, USA*

Magnesium oxide, an important component of the Earth's mantle, has been extensively studied in the pressure and temperature range found within the Earth. However, much less is known about its behavior under conditions appropriate for newly-discovered super-Earth planets, where pressures can exceed 1000 GPa (10 Mbar). It is widely believed that MgO will follow the rocksalt (B1) to cesium chloride (B2) transformation pathway commonly found for many alkali halides, alkaline earth oxides and various other ionic compounds. Static compression experiments have determined the structure of MgO to 250 GPa but have been unable to reach pressures necessary to induce the predicted transformation, resulting in large uncertainties regarding its properties under conditions relevant to super-Earths and other large planets. Here we report new dynamic x-ray diffraction measurements of ramp-compressed MgO to 900 GPa.We report evidence for the B2 phase beginning near 600 GPa, remaining stable on further compression to 900 GPa, the highest pressure diffraction data ever collected.

Modeling the interior structure and dynamics of super-Earths (dense extrasolar planets with masses up to 10-15 times that of Earth) requires knowledge regarding phase transitions, metallization, and dissociation of the appropriate materials[1–4]. The silicates that dominate the Earth's mantle likely dissociate into oxides at the extreme pressures (1000 GPa) and temperatures (5000-10000 K) existing in super-Earth mantles[5,6]. Experimental study of structures and transitions of the constituent materials under such conditions is only just beginning. Our work on the phase diagram of MgO (periclase), an end-member of the ferropericlase solid solution (Mg,Fe)O prominent in the Earth's mantle, illustrates that new experimental techniques are now available to achieve and probe pressure and temperature conditions previously accessible to theoretical simulations only.

At ambient conditions MgO assumes the rocksalt structure (NaCl-type, B1) and this phase shows an extensive stability range both in pressure and temperature[7–9]. A phase transition from the six-coordinated B1 to the 8-fold coordinated CsCl-type (B2) structure has been predicted by theoretical simulations in the 400-600 GPa range[10–14]. While a temperature anomaly on shocked MgO at about 400 GPa was recently interpreted as the B1-B2 transformation[15], no direct structural measurements exist. Theoretical predictions on crystal structures using density functional theory involve approximations and have not previously been testable by experiments at these high pressures.

This report describes a new approach to study matter in the solid state at conditions previously inaccessible in laboratory experiments. Laser-driven ramp compression was used to compress MgO to pressures of 900 GPa and its structure was determined by *in situ* x-ray diffraction to densities as

high as 8.6 g/cm^3 (ρ_0=3.58 g/cm^3, 2.4 compression). These data reveal a solid-solid phase transition at 600 GPa, and the structure of the new polymorph is consistent with the B2 phase. Simultaneous velocimetry and diffraction data are used to determine the stress-density response of MgO to 900 GPa.

Experiments were performed at the Omega Laser[16]. Targets consisted of 10-μm-thick MgO powder pressed between two diamonds. The diamond/MgO sandwich was placed on a 300-μm-diameter pinhole sitting on the front face of a diffraction diagnostic (Fig.1a)[17]. The surface of the first diamond was ablated using laser beams with intensity increasing over ∼4.5 ns, producing a ramped pressure wave (Fig.1b). Ramp loading has been shown to produce a compression path significantly cooler than shock compression, albeit hotter than isentropic compression (Supplementary Material S4). The pressure wave ultimately reaches the rear surface of the back diamond, accelerating it into free space. A velocity interferometer (VISAR)[18] records the free-surface velocity versus time, $U_{fs}(t)$. The equation of state of diamond[19] and the measured $U_{fs}(t)$ provide the stress history in MgO[17,20,21] (Fig.1c). Sandwiching MgO between diamonds ensures that diffraction samples a uniform stress state. A Cu foil was irradiated using additional lasers with a 1-ns pulse-length (Fig. 1a and b) to produce quasi-monochromatic He-α radiation (1.48 Å) incident at 45°[17]. Diffracted x-rays were recorded in transmission geometry by image plates lining the inner walls of the diagnostic box. Diffraction peaks from the edges of the pinhole provided calibration for the diffraction geometry[17].

Our experiments provide the first direct structural evidence for the occurrence of a solid-solid phase transition in MgO. Two representative diffraction images collected at 309(10) GPa and 757(63) GPa are shown in Fig. 2, together with the respective partially-integrated, one-dimensional patterns. The raw data from the image plates lining the box (Fig. 2a and b) are background-subtracted and projected into 2θ-ϕ space (where 2θ is the scattering angle and ϕ is the azimuthal angle around the incident x-ray direction, Fig. 2c and d)[17]. Two peaks from compressed MgO are visible at 309(10) GPa (highlighted by arrows), as well as reflections from the pinhole reference material (Pt) and diamond (Supplementary Material S1). The MgO diffraction peaks are consistent with the (200) and (220) lines of the B1 structure, the most intense reflections for this structure (Fig. 2e). The (200) diffraction peak for B1-MgO is observed in all the shots between ambient pressure and 563(10) GPa. The (111) and (220) reflections are sometimes observed, supporting the assignment of the MgO structure to the expected B1 phase. The measured d-spacings versus stress are reported in Fig. 3a (Supplementary Table S1) and compared with previous experimental (B1) and theoretical (B2) data. In the low-pressure phase they are in good agreement with the (111), (200) and (220) reflections obtained from extrapolation of diamond anvil cell data[7,8]. A small discontinuity in the d-spacing of the (200) reflection is observed around 420 GPa (Fig. 3a). This may be due to a distortion of the B1 unit cell or a subtle, unexpected phase transition. The change in d-spacing is not consistent with the B8 phase (NiAs structure) that has been proposed as a possible polymorph of MgO[22,23]. Non-hydrostaticity and uniaxial compression can cause lattice distortions yielding higher d-spacings than those measured under quasi-hydrostatic conditions, as observed in diamond anvil cell experiments employing similar scattering geometry (black and red curves in Fig. 3a)[7,8]. A major discontinuity in d-spacing is observed above 570 GPa and the corresponding diffraction patterns are significantly different, as shown in Fig. 2b and d at 757(63) GPa. Aside from the peaks due to diamond and the Ta reference, a new line near 2θ=63° (blue arrow) is observed. The corresponding d-spacing,

assuming a cubic structure, is consistent with the expected location of the most intense line (110) of the B2 phase of MgO at this pressure (Fig. 3a). The new pattern has been observed up to 900 GPa (Supplementary Material S2) and the assignment of the new phase to the B2 structure provides stress-density values consistent with theory[11,13,24]. Confidence in this structural identification is enhanced by the fact that the (110) peak is the most intense reflection for B2-MgO (Fig. 2c). Other structures have been tested but they do not provide a good fit to our data (Supplementary Material S3).

The density of crystalline MgO up to 900 GPa is determined by assigning the measured d-spacings to either the B1 or the B2 structure (red and blue dots respectively in Fig. 3b). Previous experimental density measurements are limited to pressures of ∼200-250 GPa for the solid phase (gas gun shock experiments[23,25–27] and static x-ray diffraction[7–9]). Our data set considerably extends the explored pressure range, reaching 2.4-fold compression for solid MgO. Fitting our data below 420 GPa to a third order equation of state (EOS), with fixed initial density and bulk modulus (ρ_0=3.58 g/cm^3 and K_0=162.5 GPa[27]), we obtain K'_0=4.1±0.2 (Supplementary Material S5 and Table S2), consistent with previous determinations of the MgO EOS. Above 563(10) GPa the three data points for the B2 phase are tentatively fitted to the same functional forms, where the initial density was fixed to the average value reported for the B2 structure (ρ_0=3.71 g/cm^3) and the bulk modulus was constrained to a range of predicted values (K_0=152.6-169.8 GPa), obtaining K'_0=4.6±0.4 (Supplementary Material S5 and Table S2). We have excluded the data between 420 and 563 GPa (empty circles in Fig. 3b) from the fit of the B1 EOS, due to the possibility of a lattice distortion. Based on our experimental data we cannot determine the nature of the distortion, so the density has tentatively been calculated assuming the B1 structure.

Recent shock experiments have shown that MgO completely melts on the Hugoniot at about 700 GPa[15]. Our observation of solid diffraction at 900 GPa clearly demonstrates that the temperature under ramp compression is lower than under shock compression. Because the diamond is opaque above 100 GPa, we cannot directly estimate the MgO temperature by pyrometry. The B1-B2 phase transformation is predicted to exhibit a negative Clapeyron slope for its coexistence[28]. Assuming $\partial P/\partial T$=-3.9±3.0×10^{-4} TPa/K[14,15], we estimate the temperature of the B1/B2 transition at 600 GPa to be less than 4000 K, about 9000 K lower than shock compression temperatures (Supplementary Material S4). These pressures and temperatures are expected to find physical realization in super-Earths with masses 5 times the mass of the Earth[1]. The experimental observation of the B2 phase of MgO and the confirmation of a negative slope for the B1/B2 coexistence line provide a benchmark for theories modeling planetary formation and evolution.

A variety of terrestrial planetary compositions are expected to occur in extrasolar planets[29]. For an Earth-like planet, (Mg,Fe)O will be an important mantle component and may be the dominant constituent in the deep interiors of larger planets for which silicate dissociation occurs above 1000 GPa[3,6]. For systems enriched in Mg/Si relative to Earth, MgO will be even more abundant. Mineralogical changes in the interior of a planet affect the pressure-density relationship and alter key physical properties. Phase transitions with a negative Clapeyron slope as in MgO can induce layered convection in the interior[30]. In contrast to the conventional view that viscosity will increase with depth, it has been proposed that the formation of abundant B2 MgO in the deep mantle of super-Earths may reduce the viscosity due to the low creep strength of B2 oxides[3]. Viscosity and

mantle convection control the thermal evolution of planets and also influence tidal heating, orbital evolution, and magnetic field generation[3]. Knowledge of phase transition behavior of MgO is thus fundamental to understanding super-Earth interiors.

In summary, we have reported the first direct experimental evidence for a solid-solid phase transition in MgO, consistent with the B1/B2 transition. This has important implications for planetary science, since these conditions are expected to exist in the deep interiors of planets over 5 times more massive than the Earth[1,2]. Our work also reports the first direct measurements of a solid-solid phase transition at these high pressures (600 GPa) and short timescales (a few ns). This opens the possibility to explore solid state behavior in materials at conditions previously inaccessible to experimental study.

---

[1] Valencia, D., O'Connell, R. J. & Sasselov, D. Internal structure of massive terrestrial planets. *Icarus* **181**, 545–554 (2006).

[2] Wagner, F. W., Tosi, N., Sohl, F., Rauer, H. & Spohn, T. Rocky super-Earth interiors. Structure and internal dynamics of CoRoT-7b and Kepler-10b. *Astronomy and Astrophysics* **541**, A103 (2012).

[3] Karato, S.-i. Rheological structure of the mantle of a super-Earth: Some insights from mineral physics. *Icarus* **212**, 14–23 (2011).

[4] Swift, D. C. *et al.* Mass-radius relationships for exoplanets. *The Astrophysical Journal* **744**, 59 (2012).

[5] Umemoto, K. & Wentzcovitch, R. M. Two-stage dissociation in $MgSiO_3$ post-perovskite. *Earth and Planetary Science Letters* **311**, 225–229 (2011).

[6] Tsuchiya, T. & Tsuchiya, J. Prediction of a hexagonal SiO_2 phase affecting stabilities of $MgSiO_3$ and $CaSiO_3$ at multimegabar pressures. *Proceedings of the National Academy of Sciences of the United States of America* **108**, 1252–1255 (2011).

[7] Duffy, T. S., Hemley, R. J. & Mao, H.-k. Equation of state and shear strength at multimegabar pressures: magnesium oxide to 227 GPa. *Physical Review Letters* **74**, 1371 (1995).

[8] Dewaele, A., Fiquet, G., Andrault, D. & Hausermann, D. P-V-T equation of state of periclase from synchrotron measurements. *Journal of Geophysical Research* **105**, 2869–2877 (2000).

[9] Dorfman, S. M., Prakapenka, V. B., Meng, Y. & Duffy, T. S. Intercomparison of pressure standards (Au, Pt, Mo, MgO, NaCl and Ne) to 2.5 Mbar. *Journal of Geophysical Research* **117**, B08210 (2012).

[10] Strachan, A., Çagin, T. & Goddard, W. A. Phase diagram of MgO from density-functional theory and molecular-dynamics simulations. *Physical Review B* **60**, 15084–15093 (1999).

[11] Mehl, M. J., Cohen, R. E. & Krakauer, H. Linearized augmented plane wave electonic structure calculation for MgO and CaO. *Journal of Geophysical Research* **93**, 8009–8022 (1988).

[12] Drummond, N. & Ackland, G. Ab initio quasiharmonic equations of state for dynamically stabilized soft-mode materials. *Physical Review B* **65**, 184104 (2002).

[13] Oganov, A. R., Gillan, M. J. & Price, G. D. Ab initio lattice dynamics and structural stability of MgO. *Journal of Chemical Physics* **118**, 10174 (2003).

[14] Belonoshko, A. B., Arapan, S., Martonak, R. & Rosengren, A. MgO phase diagram from first principles

in a wide pressure-temperature range. *Physical Review B* **81**, 054110 (2010).

[15] McWilliams, R. S. *et al.* Phase transformations and metallization of magnesium oxide at high pressure and temperature. *Science* **338**, 1330 (2012).

[16] Boehly, T. R. *et al.* Initial performance results of the OMEGA laser system. *Optics Communication* **133**, 495–506 (1997).

[17] Rygg, J. R. *et al.* Powder diffraction from solids in the terapascal regime. *Review of Scientific Instruments* **83**, 113904 (2012).

[18] Celliers, P. M. *et al.* Line-imaging velocimeter for shock diagnostics at the OMEGA laser facility. *Review of Scientific Instruments* **75**, 4916 (2004).

[19] Bradley, D. K. *et al.* Diamond at 800 GPa. *Physical Review Letters* **102**, 075503 (2009).

[20] Maw, J. R. A characteristics code for analysis of isentropic compression experiments. *AIP Conference Procedings* **706**, 1217–1220 (2004).

[21] Rothman, S. D. & Maw, J. Characteristics analysis of isentropic compression experiments (ICE). *J. Phys. IV France* **134**, 745–750 (2006).

[22] Causà, M., Dovesi, R., Pisani, C. & Roetti, C. Electronic structure and stability of different crystal phases of magnesium oxide. *Physical Review B* **33**, 1308 (1986).

[23] Zhang, L., Gong, Z. & Fei, Y. Shock-induced phase transitions in the MgO-FeO system to 200GPa. *Journal of Physics and Chemistry of Solids* **69**, 2344–2348 (2008).

[24] Bukowinski, M. S. T. First principles equations of state of MgO and CaO. *Geophysical Research Letters* **12**, 536 (1985).

[25] Marsh, S. *LASL Shock Hugoniot Data* (University Califorina Press, Berkeley, 1980).

[26] Vassiliou, M. S. & Ahrens, T. J. Hugoniot equation of state of periclase to 200 GPa. *Geophysical Research Letters* **8**, 729–732 (1981).

[27] Duffy, T. S. & Ahrens, T. J. Compressional sound velocity, equation of state, and constitutive response of shock-compressed magnesium oxide. *Journal of Geophysical Research* **100**, 529–542 (1995).

[28] Wu, Z. *et al.* Pressure-volume-temperature relations in MgO: An ultrahigh pressure-temperature scale for planetary sciences applications. *Journal of Geophysical Research* **113**, 1–12 (2008).

[29] Bond, J. C., O'Brien, D. P. & Lauretta, D. S. The compositional diversity of extrasolar terrestrial planets. I. In situ simulations. *The Astrophysical Journal* **715**, 1050–1070 (2010).

[30] van den Berg, A. P., Yuen, D. A., Beebe, G. L. & Christiansen, M. D. The dynamical impact of electronic thermal conductivity on deep mantle convection of exosolar planets. *Physics of the Earth and Planetary Interiors* **178**, 136–154 (2010).

Supplementary Information is linked to the online version of the paper at www.nature.com/nautre.

Acknowledgements The authors thank Stephanie Uhlich, Walter Unites and Timothy Uphaus for their assistance in target preparation and the operation staff at the OMEGA laser facility for supporting these experiments. F.C. is grateful to D. C. Swift for providing a tabular equation of state of MgO. The authors thank R. E. Cohen and M. J. Mehl for discussions and for making simulation results available. This work was performed under the auspices of the U. S. Department of Energy by Lawrence Livermore National Laboratory under Contract No. DE-AC52-07NA27344. The research was supported by NNSA/DOE through the National Laser Users' Facility Program under contracts DE-NA0000856 and DE-FG52-09NA29037.

Author Contributions F.C. was the primary person who designed and performed the experiment, analyzed the data and wrote the manuscript. R.F.S., J.H.E. and T.S.D assisted in the design and performance of the experiment and contributed to the manuscript. J.W. assisted in the design and performance of the experiment. J.R.R., A.L. and J.A.H. participated in the design of the experiment. G.W.C. participated in the design of the experiment and contributed to the manuscript. All the authors discussed the results together and commented on drafts of the manuscript.

Author Information The authors declare no competing financial interests. Reprints and permissions information is available at www.nature.com/reprints. Correspondence and requests for materials should be addressed to F.C. (coppari1@llnl.gov).

FIG. 1. Experimental setup and results. (**a**) Schematic representation of the diagnostic used for ramp-compression x-ray diffraction measurements. The target assembly (detail in the zoomed region) consists of a MgO layer sandwiched between two single-crystal diamonds centered over a Pt or Ta pinhole. This package sits in the front plate of a box containing image plates that record the diffraction signal. The collimated direct x-ray beam hits the bottom plate and diffracted x-rays are recorded on the other panels of the box (the red lines illustrates an example diffraction line of constant 2θ=55°). A source of x-rays with dominant wavelength of 1.48 Å is generated by laser illumination of a Cu foil. Four additional laser beams are used to drive the target to high pressure. The box has a hole in the back panel to allow simultaneous VISAR measurements for pressure determination. (**b**) The ramped pulse shape (red curve) used to drive the target is shown together with the 1-ns pulse (black curve) used to drive the x-ray source (XRS). (**c**) The measured free surface velocity (black) and the stress history in the MgO layer (red) are shown as a function of time.

FIG. 2. X-ray diffraction patterns of compressed MgO. (**a**) Raw diffraction pattern for B1-MgO at 309(10) GPa. The red arrow highlights the diffraction peak from the MgO, crosses indicate the lines from the reference material (Pt) and "C" indicates diffraction peak from the diamond. (**b**) Raw diffraction pattern for the new phase of MgO at 757(63) GPa. The new peak from MgO is highlighted by a blue arrow, triangles indicate the Ta reference lines and "C" the diamond peak. (**c**)-(**d**) The raw data in panel (a) and (b) are converted into 2θ-ϕ space and the corresponding integrated intensity are shown below the two-dimensional images. In panel (c) the (200) and (220) reflections for B1-MgO are visible (red arrows) in addition to lines from the reference Pt and textured peaks from the diamond (indicated by crosses and the label "C" in the integrated one-dimensional pattern). In panel (d) a peak consistent with the (110) reflection of the B2 structure is visible at 2θ=63° (blue arrow) and no diffraction peaks from the B1 phase are observed. Peaks from diamond ("C") and Ta reference (triangles) are also observed. In both panels dashed regions indicate the portion of the image integrated to obtained the one-dimensional pattern. The expected 2θ values of all the reflections of B1 and B2 MgO occurring in the explored angular range are indicated. The observed peaks are highlighted by arrows in the 2θ-ϕ images and by colored peaks in the one-dimensional patterns. (**e**) Expected relative intensity for the diffraction peaks of B1 (at 309 GPa) and B2 (at 757 GPa) MgO.

FIG. 3. Measured d-spacings and density of MgO to 887(62) GPa. (**a**) d-spacings vs stress. We observe reflections consistent with the B1 structure up to 414(15) GPa and our results are in good agreement with extrapolations from diamond anvil cell experiments[7,8]. A small discontinuity is observed above 420 GPa, possibly due to lattice distortion. Above 563(10) GPa a major discontinuity in the d-spacing indicates the onset of a phase transition. The assignment of the observed peak to the (110) reflection for the B2 structure results in density values consistent with simulations (blue and black dashed lines from linearized augmented plane wave electronic structure and density functional theory calculations, respectively)[11,13]. (**b**) Density of MgO obtained by fitting the d-spacing to the B1 (red dots) or B2 (blue dots) structure. The density reported between 400 and 600 GPa (empty dots) is calculated assuming the B1 structure (see text for details). Also shown are data from gas gun[23,25–27] and laser shock experiments[15]. Continuous red and blue lines are fit to our data (see text

and Supplementary Material S5).

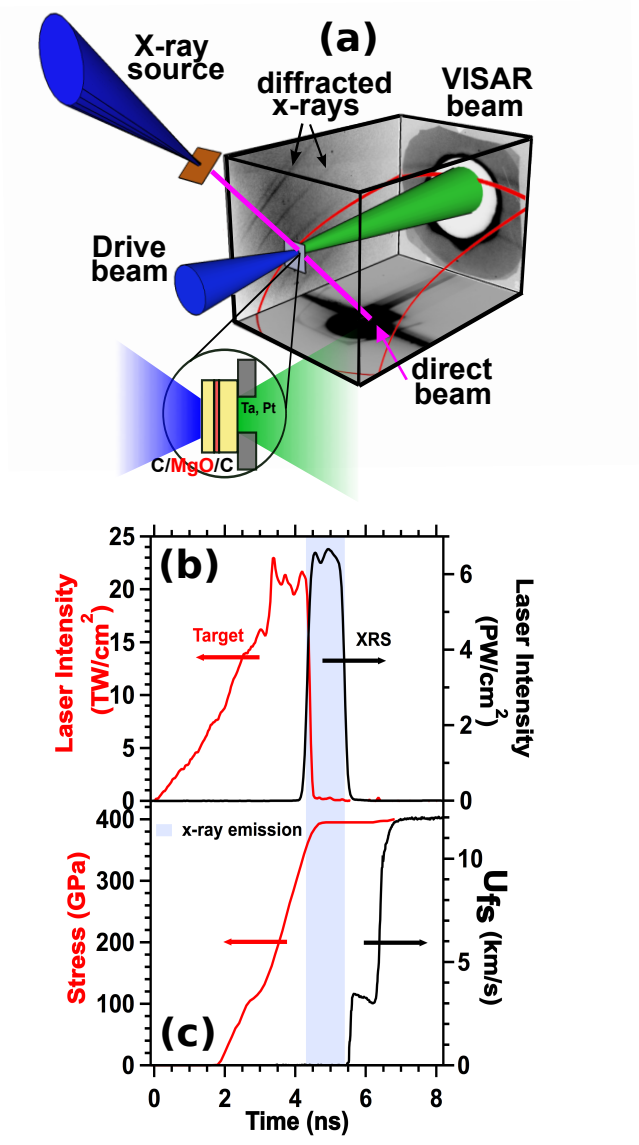
(a)
X-ray source
diffracted x-rays
VISAR beam
Drive beam
direct beam
Ta, Pt
C/MgO/C
(b)
Laser Intensity (TW/cm^2)
Laser Intensity (PW/cm^2)
Target
XRS
x-ray emission
(c)
Stress (GPa)
U_{fs} (km/s)
Time (ns)

(a)
309(10) GPa
C
(b)
757(63) GPa
C
309(10) GPa
(c)
100
0
-100
ϕ (°)
B1 111
B1 200
B1 220
B1 311
B1 222
C
757(63) GPa
(d)
100
0
-100
ϕ (°)
B2 100
C
B2 110
B2 111
B2 200
C
B2 210
B1
B2
Rel. Int.
(e)
40
60
80
100
2θ (°)

(a)

This work
XRD, non-hydrostatic DAC:
data extrapolation
XRD, quasi-hydrostatic DAC:
data extrapolation
B2 EOS from simulations:
LAPW
DFT

(111)
(200)
(220)
(110)

d-spacing (Å)

(b)

This work: B1 B2
B1 fit B2 fit
Gas Gun shock (B1)
Laser shock (liquid)

B1 → B2

Density (g/cm^3)

Stress (GPa)

SUPPLEMENTARY DISCUSSION AND FIGURES

S1. Diffraction from diamond

Peaks from the diamond layers are observed in our x-ray diffraction measurements. The strong uniaxial compression wave breaks the symmetry of the single crystal diamond resulting in distorted peaks shapes. Since the diamond experiences a large pressure gradient in these experiments [1], diffraction peaks can correspond to a range of pressure, from ambient up to the peak pressure. This generates diamond diffraction peaks with a unique character that is qualitatively different from the signal of the more uniformly compressed MgO. As can be observed in Fig. S1 the peak associated with the (111) reflection of diamond (highlighted in the inset) has a wider 2θ extension and a smaller extension in azimuthal angle ϕ than the MgO peaks. The specific character of the diamond peaks made the assignment of the MgO reflections unambiguous.

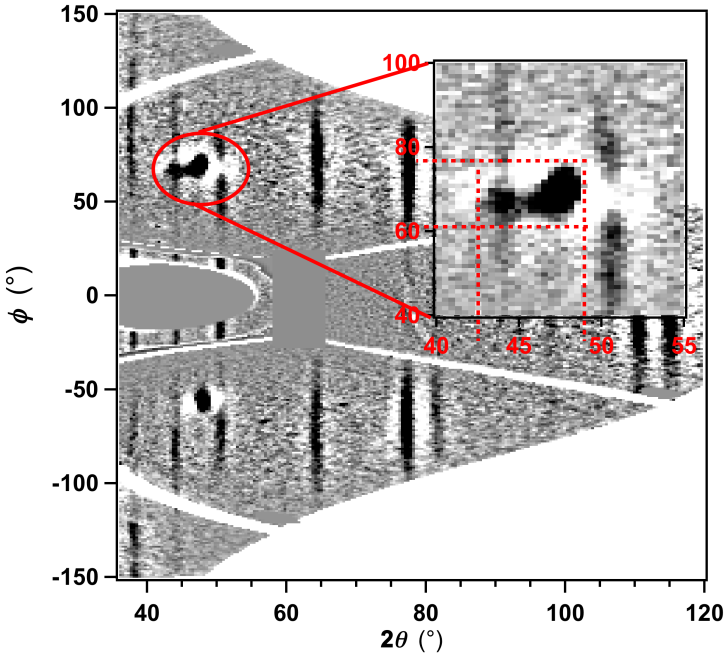

FIG. S1. *Diffraction pattern of MgO sandwiched between two single-crystal diamonds ramp compressed to 309(10) GPa. Peaks from the reference material (Pt) and from compressed MgO and diamond are visible. The compression-induced texture and the pressure gradient in the diamond result in diffraction peaks characterized by a broader 2θ range and smaller ϕ range.*

S2. Raw data for the high pressure phase of MgO

The following figure shows the raw data (before transformation to the usual ϕ-2θ space) for the three shots taken above 600 GPa and showing the absence of the (200) line for B1-MgO and the appearance of a new peak (highlighted by arrows in each panel). This peak has been observed in every shot where MgO was ramp-compressed above 600 GPa and it shows a shift as a function of pressure consistent with equations of state of B2-MgO.

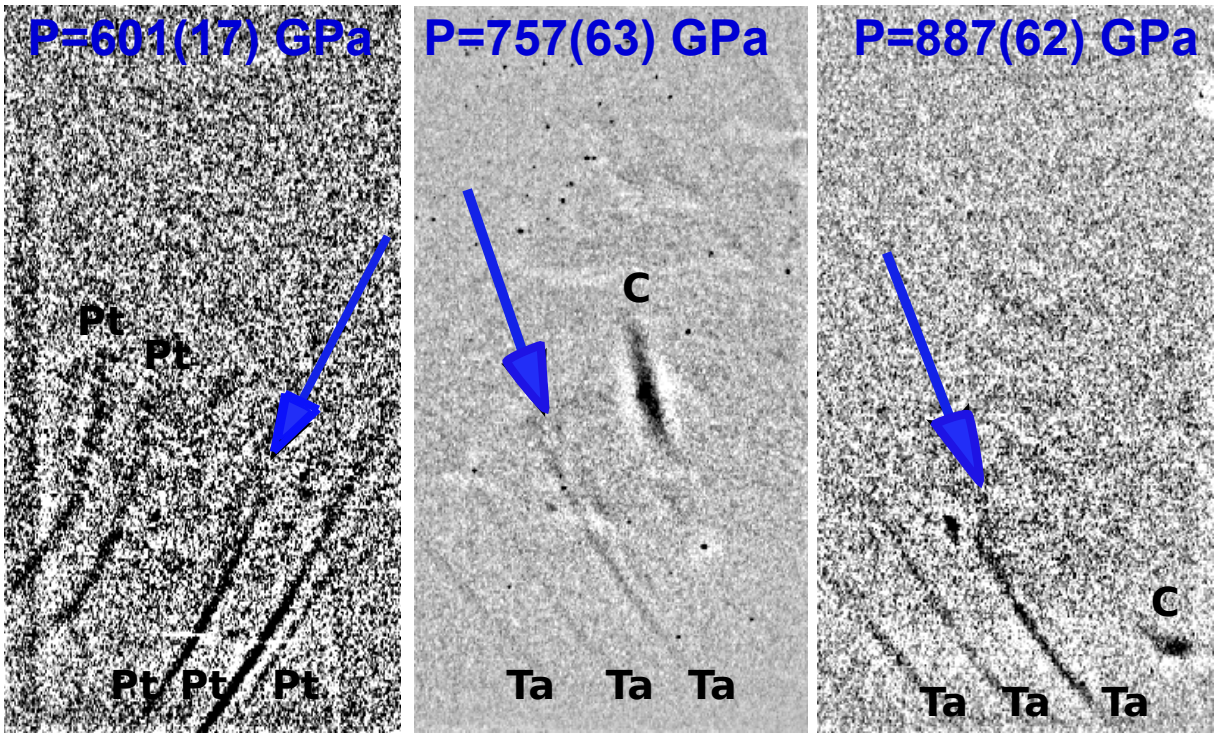

FIG. S2. *Raw diffraction images for MgO in the high pressure phase. The new peak from MgO (highlighted by arrows) has been observed in all the shots above 600 GPa. The extra lines are from the reference material ("Pt" or "Ta" labels) and diamond ("C" labels).*

S3. High pressure MgO polymorphs

The identification of the high pressure phase of MgO as B2 is the one that provides the best agreement with theoretical simulations of the high pressure EOS of MgO and a reasonable evolution of density as a function of pressure. Other possible MgO polymorphs may exist, even though theoretical simulations [2–5], including random structure search [7], find the B2 structure to be the stable one at high pressure.

In order not to neglect any possibility we have fit our data to these structures looking for other possible agreement with our experiment.

In the following a brief description of each proposed polymorph for MgO is reported, and the expected d-spacings against pressure are compared to the experimental data:

- **B2-CsCl structure:** B2-MgO has the CsCl structure, with cubic unit cell ($Pm3m$) and 2 atoms/unit cell. Ab-initio simulations and random structural search calculation predict MgO to assume this structure at high pressure [2, 3, 6, 7]. Using the theoretical EOS from ref. [2, 3] we calculated the expected d-spacing for B2-MgO as a function of pressure and the result is reported in Fig. S3. There is excellent agreement between the position of the (110) peak of B2-MgO and the measured d-spacing above 600 GPa.

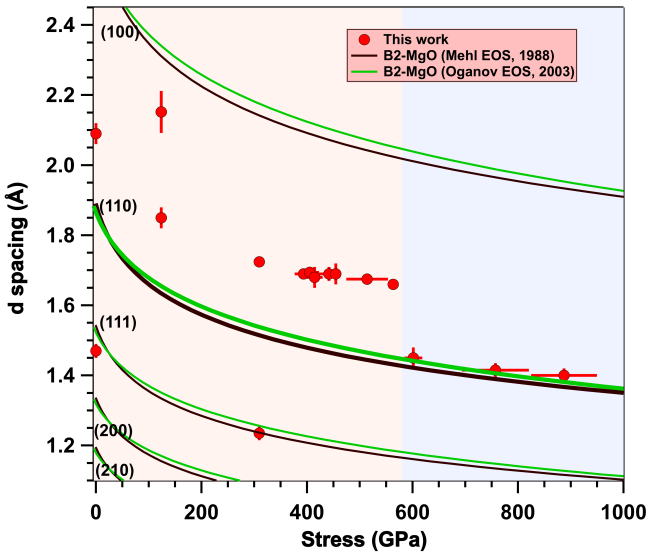

FIG. S3. *Comparison of our measured d-spacing with those expected for B2-MgO using EOS from ref. [2, 3]. The strongest reflection for this structure is the (110) and it is highlighted by thicker lines.*

- **B8-NiAs structure:** The B8 phase of MgO would have the NiAs-type structure, with hexagonal unit cell ($P6_3/mmc$) and 4 atoms/unit cell. Early *ab-initio* simulations predict this structure to be stable and energetically competitive with the B1 around 2 Mbar [8]. Using theoretical EOS for this structure [8, 9] (green and black lines in Fig. S4) we calculate the expected d-spacings and compare the results with the observed diffraction peaks. As can be observed in Fig. S4 this structure has no peak that agrees with our experimental data.

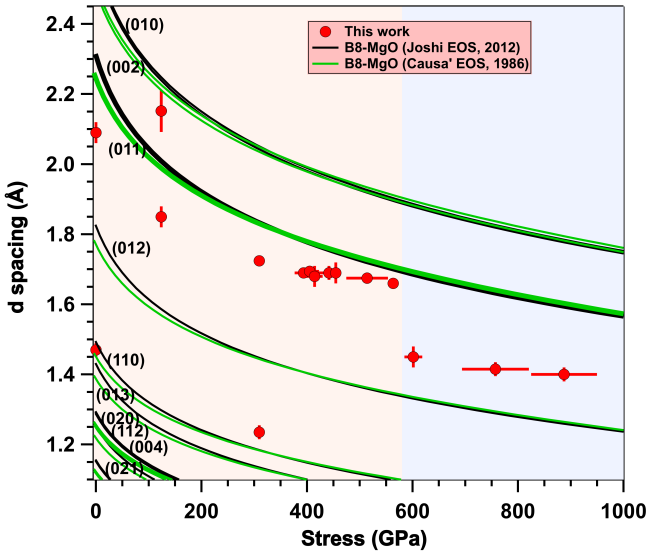

FIG. S4. *Comparison of our measured d-spacing with those expected for B8-MgO. The thickest lines representing the (011) peak indicate the most intense reflection for this structure.*

- **B3-ZnS structure:** In the B3 phase MgO would have the zincblende structure ($F43m$) with 8 atoms/unit cell and a face-center-cubic (fcc) lattice. The coordination number for this structure is 4 (lower than the 6-fold coordination of B1 MgO) and therefore it is unlikely to observe this phase at high pressure as a transformation from the B1. As can be observed in Fig. S5, the (200) line for B3-MgO is the one that is closer to our experimental data, but its extrapolation above 600 GPa using the EOS from [9] is not consistent with the experimentally observed diffraction peaks.

- **B4-ZnS structure:** B4-MgO would have the wurtzite structure, with a hexagonal lattice ($P6_3mc$) and 4 atoms/unit cell. Again, this structure is characterized by coordination 4, lower than the ambient pressure phase of MgO. Two equations of state for this structure have been used to extrapolate the d-spacing at high pressure ([9, 10]) but there is no agreement with the experimental ones (Fig. S6).

- **h-BN:** This is the hexagonal boron nitride structure ($P6_3/mmc$) with 4 atoms/cell and coordination 3. Equations of state for MgO in the h-BN structure (h-MgO) have been calculated and reported in [9, 10] and they are compared to our experimental data in Fig. S7. The (002) line for h-MgO is somewhat close to our experimental data above 600 GPa (at least using the EOS from [9]). However if we assume a transformation from B1 to h-MgO (that would imply a transformation to a more open structure as a function of pressure) one would have a density increase of 22%

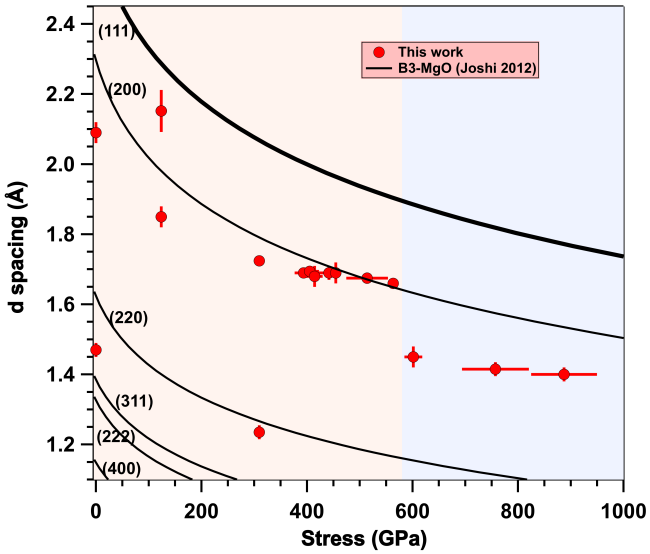

FIG. S5. *Comparison of our measured d-spacing with those expected for B3-MgO. The (111) peak of B3-MgO is the most intense reflection (thick line).*

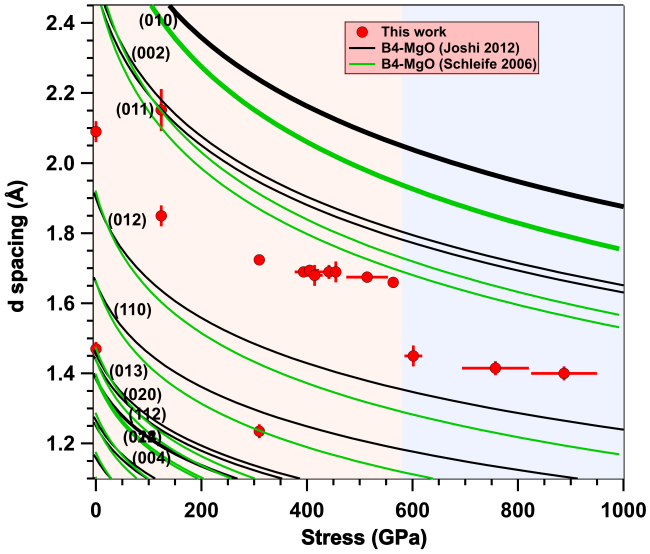

FIG. S6. *Comparison of our measured d-spacing with those expected for B4-MgO using EOS from [9, 10]. The most intense reflection for this structure is the (101) (thick lines).*

at the transition (see yellow triangles in Fig. S10 in the final discussion), which is not reasonable.

- **t-MgO_2:** New stoichiometries in the Mg-O systems have been predicted to occur in Mg-O compounds at high pressure [11]. In particular, a tetragonal phase of magnesium peroxide (t-MgO_2)

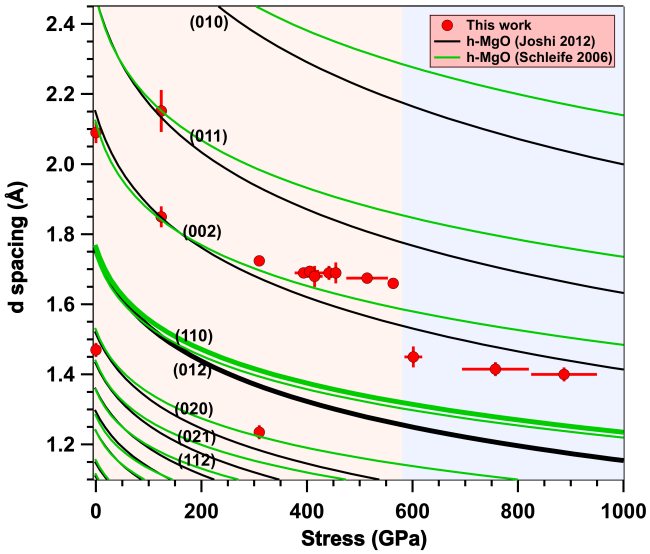

FIG. S7. *Comparison of our measured d-spacing with those expected for h-MgO. The most intense reflection is the (110) indicated by thicker lines.*

has been predicted to be stable above 500 GPa. This structure (space group $I4/mcm$) has 12 atoms/unit cell and the Mg is 8-fold coordinated. Using the lattice parameters reported in [11] we calculate the d-spacings for this structure at 500 GPa (squares in Fig. S8). If one assumes that the experimentally observed peaks are the (112) for t-MgO_2 at higher compression, the MgO would experience an even more dramatic density jump across the transition (∼25%, see Fig. S10, gray squares).

- **t-Mg_3O_2:** Another exotic stoichiometry predicted to occur at high pressure [11] is the tetragonal Mg_3O_2 (t-Mg_3O_2). This structure belongs to the $P4/mbm$ space group and counts 10 atoms/unit cell. The t-Mg_3O_2 appears to be stable above 500 GPa. Using the lattice parameters at 500 GPa reported in [11] we calculated the d-spacings expected for this structure (triangles in Fig. S9). Again, if we assume that the experimental peaks are the (121) line, the density jump across the transition would be 11% (Fig. S10, gray triangles).

Summarizing, different structures have been used to fit our experimental d-spacings. Those that could have d-spacings reasonably close to the observed ones are h-MgO, t-MgO_2 and t-Mg_3O_2. However the corresponding density for that structure would be much higher that what one can get by fitting the experimental data with the B2 structure and would have to assume a density jump of at least 11% (for t-Mg_3O_2).

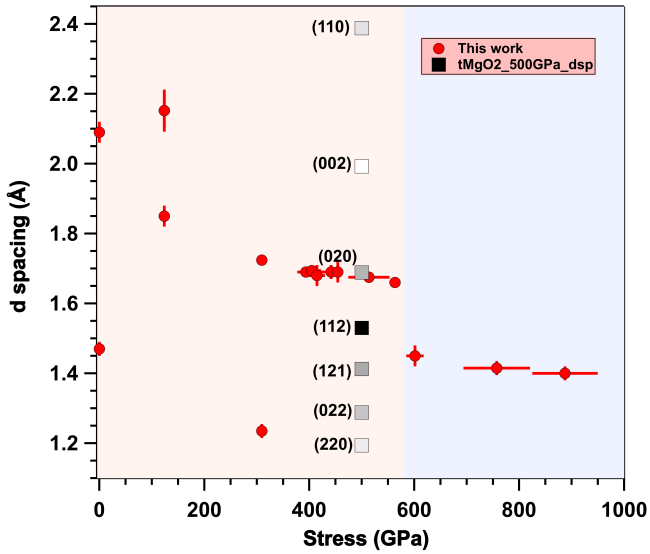

FIG. S8. *Comparison of our measured d-spacing with those expected for t-MgO_2 at 500 GPa. The gray scale of the symbols is associated with the relative intensity of the peaks (black to white corresponds to high to low). The most intense peak for this structure is the (112).*

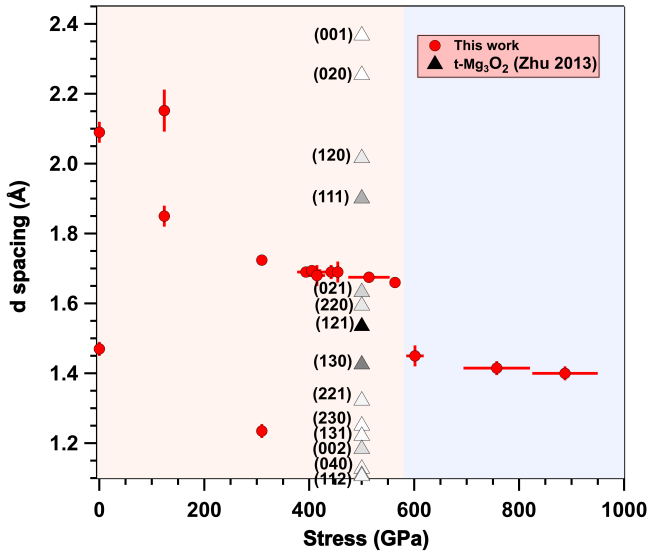

FIG. S9. *Comparison of our measured d-spacing with those expected for t-Mg_3O_2 at 500 GPa. The gray scale of the symbols is associated with the relative intensity of the peaks, from high (black) to low (white). The most intense peak for t-Mg_3O_2 is the (121).*

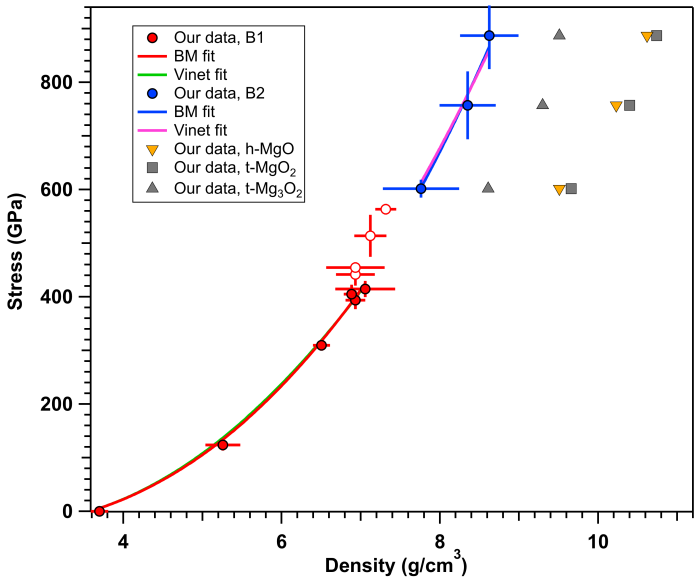

FIG. S10. *Stress-density plot for MgO assuming different high pressure structures. Data below 600 GPa have been fitted to the B1 structure. Above 600 GPa blue dots indicate the density assuming a transition to the B2-MgO, yellow triangles are for h-MgO, gray squares indicate the density for t-MgO_2 and gray triangles are the density for t-Mg_3O_2.*

S4. Thermodynamic path in ramp-compression technique

Shock and ramp compression experiments probe different thermodynamic states. Temperatures reached in ramp loading are expected to be lower than those obtained along the shock Hugoniot (the locus of final states accessible via a planar shock) and hotter than the isentrope [12]. Recent experiments confirmed that this is the case [13]. Energy, density and pressure in a shock experiment are related by the Rankine-Hugoniot equations and the temperature reached is directly related to the obtained energy [12]. For ramp compression the pressure-density-temperature relationship is not well defined. In our diffraction experiments we cannot measure the temperature using pyrometry, because the diamond window becomes opaque when compressed above 100 GPa [14], making any measurement of the emission from the MgO layer impossible. Nevertheless, certain assumptions can be made to bound the temperature of MgO under ramp compression. In Fig. S11 we consider a typical free surface velocity profile (peak stress of 393(17) GPa) which exhibits a multiple wave structure, where the first rise in velocity, associated with the diamond elastic wave, is followed by the main plastic deformation wave and a final more gentle ramp to the peak velocity. An upper bound for the temperature reached in our measurements can be estimated if we assume that the MgO experiences a double shock, instead of

the observed ramps in the data record. In this analysis, the first and second compression waves would correspond to a 60 GPa initial shock and a 300 GPa secondary shock within the MgO layer. Using a tabular multiphase equation of state for MgO [15] we then estimate the temperature states associated with the double shock. In T-P space, the initial 60 GPa shock lies along the principal Hugoniot (red curve in Fig. S12) at a temperature of ∼700 K. The second 300 GPa shock lies along the secondary Hugoniot (orange curve) at ∼2700 K. As indicated in Fig. S11 the final compression above the second shock is through ramp compression. In T-P space we approximate this portion of the drive with an isentrope starting at the second shock state (light blue curve calculated from 300 GPa and 2700 K). The lower bound to the temperature is the room temperature isentrope (dark blue curve). Therefore for the 393(17) GPa shot the temperature in the MgO is bounded between the temperature limits indicated by the blue arrow in Fig. S12. The same methodology was applied to all the experimental points we collected and the temperature bounds are represented in Fig. S12 through the gray shaded area.

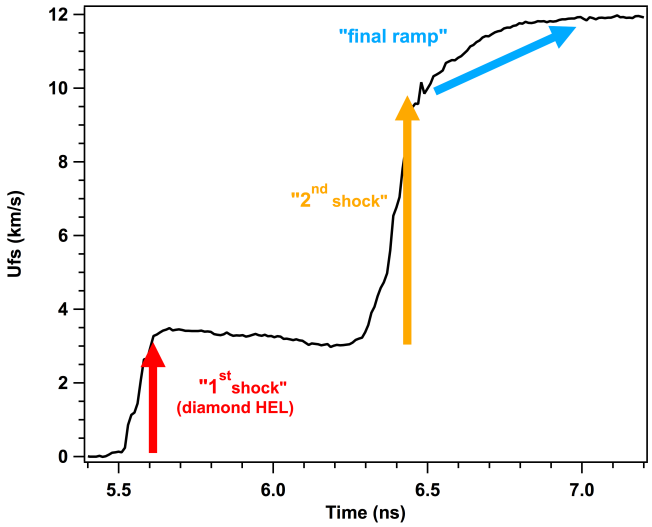

FIG. S11. *Free surface velocity measured in the shot to 393(17) GPa. To estimate an upper bound for the temperature of the MgO layer we assume that the two wave structure in the free surface velocity are due to shocks (red and orange arrows corresponding to the elastic and plastic wave of diamond, respectively), followed by a final ramp to the peak free surface velocity (light blue arrow, see text for details).*

Considering the Clapeyron slope for the B1/B2 transition reported in [16] we can estimate the temperature at the transition pressure observed in our experiments (600 GPa). Assuming that the phase boundary is represented by a straight line of slope $\partial T/\partial P$=-26±30 K/GPa ([4, 16], purple dashed line in Fig. S12), we obtain a temperature of about 3900±2000 K (indicated by the purple dot), where the uncertainty is given by the upper and lower bounds discussed above.

At 600 GPa our data is ∼15% denser than the values reported for shock compression: we measure ρ_R=7.76±0.48 g/cm^3 for B2-MgO at 601(17) GPa versus ρ_H=6.82±0.34 g/cm^3 for liquid MgO at about the same pressure ([16] and yellow squares in Fig. 3b). Here the subscripts "R" and "H" refer to "ramp" and "Hugoniot", respectively. Assuming that the density change between the ramp and the shock experiment is due to the heating only and using an extrapolated value for the thermal expansion coefficient we could potentially estimate the temperature reached in our ramp compression at 600 GPa (here we neglect the latent heat associated with the solid-liquid transition, this is however a small contribution, since the density change due to the melting has been reported to be only 1% [16]). Unfortunately the uncertainty associated with the density measurements in both ramp and shock compression, plus the uncertainty in the extrapolation of the thermal expansivity of MgO, do not allow to constrain the temperature obtained in our experiment.

Scattered values for the thermal expansion coefficient at high pressure and temperature have been reported, ranging from 10-11×10^{-6} K^{-1} [17, 18] to 14-16×10^{-6} K^{-1} [19] around 200 GPa and 3000 K. Extrapolation of these values to 600 GPa give 7-12×10^{-6} K^{-1} with average value α=9.5±2.5×10^{-6} K^{-1}. Using the expression:

$$\alpha = \frac{ln(\rho_R/\rho_H)}{T_H - T_R}$$

we can solve for T$_R$ (T$_H$=14100±1100 K is the temperature reached in shock compression to 600 GPa [16]), obtaining T$_R$=500±9200 K.

S5. Stress-density fit

In order to compare the density obtained in our diffraction experiments with the values reported in literature, we fit our stress-density data to two of the most used functional forms for the stress-density relations, the third order Birch-Murnaghan (BM) and Vinet equations of state [22, 23], reported below:

$$P(\rho) = \frac{3}{2}K_0\left[\left(\frac{\rho}{\rho_0}\right)^{7/3} - \left(\frac{\rho}{\rho_0}\right)^{5/3}\right]\left(1 + \frac{3}{4}\left[K_0' - 4\right]\left[\left(\frac{\rho}{\rho_0}\right)^{2/3} - 1\right]\right)$$

$$P(\rho) = 3K_0\frac{1 - \left(\frac{\rho_0}{\rho}\right)^{1/3}}{\left(\frac{\rho_0}{\rho}\right)^{2/3}}\exp\left[\frac{3}{2}\left(K_0' - 1\right)\left(1 - \left(\frac{\rho_0}{\rho}\right)^{1/3}\right)\right]$$

where ρ_0 is the initial density, K$_0$ is the bulk modulus and K$_0'$=$\left(\frac{\partial K_0}{\partial P}\right)$ is the partial derivative of the bulk modulus at ambient pressure. Due to limited number of experimental points we fixed some parameters to known values (Table S2). For the fit of the B1 structure the initial density was set to 3.58 g/cm^3 and

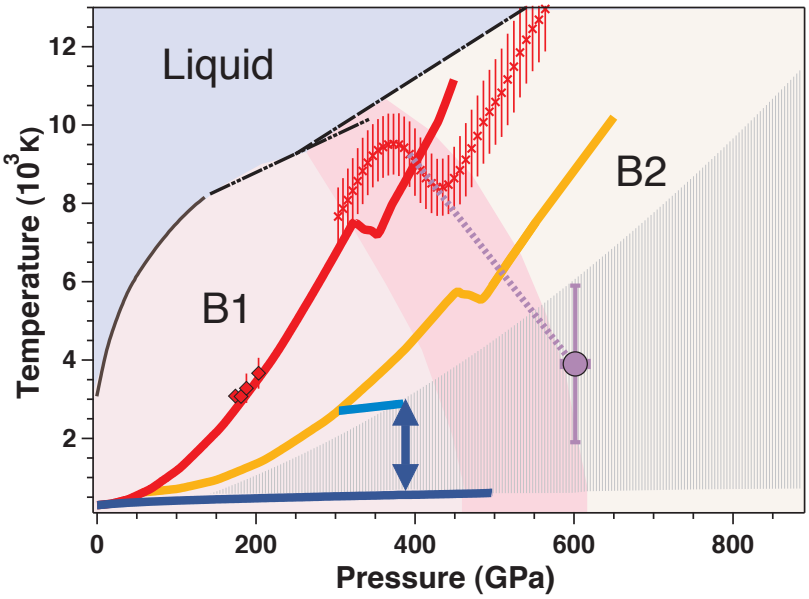

FIG. S12. *Phase diagram of MgO showing the path followed in ramp-compression experiments. The red, orange and dark blue lines are the calculated principal and the secondary Hugoniot and the isentrope curves respectively [15]. The discontinuities correspond to the B1/B2 transition. Experimental shock data are represented by crosses [16] and diamonds [20]. The black lines are calculated melting curves (continuous and dot-dashed from [4, 21]). The pink region between 400 and 600 GPa encloses the T-P region where most theoretical works locate the B1/B2 transition [3–5]. The blue arrow at 393 GPa represents the estimated temperature limits of the MgO for the shot discussed in this section (see text for details). The gray shaded region encompasses the range of possible temperature states sampled in our ramp-compression measurements. The purple dot is the estimated temperature in our ramp-compression to 600 GPa as obtained from the Clapeyron slope reported in [16].*

K_0=162.5 GPa (adiabatic bulk modulus [24]). We obtain K_0'=4.1±0.2, where the uncertainty reflects difference between Birch-Murnahan or Vinet EOS fits to the data (Table S2). For the B2 structure density and bulk modulus were constrained to values obtained from theoretical simulations. ρ_0 was fixed to the average of calculated initial densities (ρ_0=3.71 g/cm^3 [2, 3, 5, 6]) and the bulk modulus was let vary within a range of values reported in [2, 3, 5, 6] (Table S2). Again, only the pressure derivative of the bulk modulus was allowed to vary. The fit gives K_0'=4.6±0.4 and the uncertainty accounts for the scatter in the fit results when using the BM or the Vinet functional forms and the different values of the fixed parameters. The fits and the corresponding residuals are reported in Fig. S13. The purpose of these fits is to provide qualitative information on how the MgO density is expected to change at ultra-high

pressure. A more rigorous fit should take into account thermal effects on the measured d-spacings.

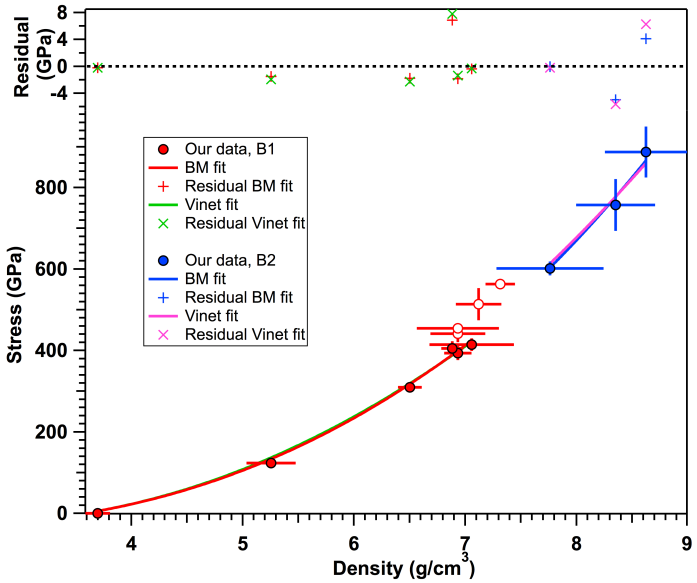

FIG. S13. *Our experimental stress-density data (red, blue and empty dots) fitted to the BM (red and blue curves for B1 and B2, respectively) and Vinet (green and pink curves for B1 and B2) EOSs. The residuals of the fits are reported in the upper panel.*

SUPPLEMENTARY TABLES

P(GPa)	d_{111} (Å)	d_{200} (Å)	d_{220} (Å)	d_{110} (Å)	Structure	ρ (g/cc)
0		2.09(3)	1.47(2)		B1	3.7(1)
124(10)	2.15(6)	1.85(3)			B1	5.2(2)
309(10)		1.72(1)	1.23(2)		B1	6.5(1)
393(17)		1.69(1)			B1	6.9(1)
405(17)		1.694(8)			B1	6.88(9)
414(15)		1.68(3)			B1	7.0(4)
441(21)		1.69(2)			B1?	6.9(2)
454(10)		1.69(3)			B1?	6.9(4)
514(39)		1.67(2)			B1?	7.1(2)
563(10)		1.66(1)			B1?	7.3(1)
601(17)				1.45(3)	B2	7.8(5)
757(63)				1.41(2)	B2	8.3(3)
887(62)				1.40(2)	B2	8.6(4)

TABLE S1. *d-spacings of MgO at high pressure measured in the diffraction experiments and corresponding density obtained by fitting the structure to the cubic B1 or B2. Numbers in parenthesis are the uncertainty on the last digit(s). The uncertainty in the P accounts for the temporal and spacial non-uniformity of the pressure in the MgO layer at the time the diffraction is collected and for the uncertainty in the measured free-surface velocity. The uncertainty in ρ is evaluated by propagation of the error in the measured d-spacing, that accounts for the uncertainty in the position of the image plates into the box and in the position of the diffraction peak's centroid. More details are given in [1].*

	B1	B2
ρ (g/cc)	3.58 (fixed)	3.71 (fixed)
K_0 (GPa)	162.5 (fixed)	152.6-169.8(fixed)
K'	4.1(2)	4.6(4)

TABLE S2. *Parameters of the MgO equation of state. The density of MgO up to 887(62) GPa has been fitted to the Birch-Murnaghan and Vinet EOSs and estimates of the fitting parameters are reported. Numbers in parenthesis are the uncertainty on the last digit. They account for the spread in the fit results when using the BM or Vinet EOS.*

[1] Rygg, J. R. *et al.* Powder diffraction from solids in the terapascal regime. *Review of Scientific Instruments* **83**, 113904 (2012).

[2] Mehl, M. J., Cohen, R. E. & Krakauer, H. Linearized augmented plane wave electonic structure calculation for MgO and CaO. *Journal of Geophysical Research* **93**, 8009–8022 (1988).

[3] Oganov, A. R., Gillan, M. J. & Price, G. D. Ab initio lattice dynamics and structural stability of MgO. *Journal of Chemical Physics* **118**, 10174 (2003).

[4] Belonoshko, A. B., Arapan, S., Martonak, R. & Rosengren, A. MgO phase diagram from first principles in a wide pressure-temperature range. *Physical Review B* **81**, 054110 (2010).

[5] Jaffe, J. E., Snyder, J. A., Lin, Z. & Hess, A. C. LDA and GGA calculations for high-pressure phase transitions in ZnO and MgO. *Physical Review B* **62**, 1660–1665 (2000).

[6] Bukowinski, M. S. T. First principles equations of state of MgO and CaO. *Geophysical Research Letters* **12**, 536 (1985).

[7] Wilson, H. & Militzer, B. Rocky Core Solubility in Jupiter and Giant Exoplanets. *Physical Review Letters* **108**, 111101 (2012).

[8] Causa, M., Dovesi, R., Pisani, C. & Roetti, C. Electronic structure and stability of different crystal phases of magnesium oxide. *Physical Review B* **33**, 1308 (1986).

[9] Joshi, K. B., Sharma, B. K., Paliwal, U. & Barbiellini, B. Pressure-dependent electronic properties of MgO polymorphs: a first-principles study of Compton profiles and autocorrelation functions. *Journal of Materials Science* **47**, 7549–7557 (2012).

[10] Schleife, A., Fuchs, F., Furthmüller, J. & Bechstedt, F. First-principles study of ground- and excited-state properties of MgO, ZnO, and CdO polymorphs. *Physical Review B* **73**, 245212 (2006).

[11] Zhu, Q., Oganov, A. R. & Lyakhov, A. O. Novel stable compounds in the Mg-O system under high pressure. *Physical chemistry chemical physics : PCCP* **15**, 7696–700 (2013).

[12] Zel'dovich, Y. & Raizer, Y. P. *Physics of Shock Waves and High-Temperature Hydrodynamic Phenomena* (Academic Press Inc., New York, 1966).

[13] Ping, Y. *et al.* Solid iron compressed up to 560 GPa. *under review* (2013).

[14] Bradley, D. K. *et al.* Shock Compressing Diamond to a Conducting Fluid. *Physical Review Letters* **93**, 195506 (2004).

[15] Drummond, N. & Ackland, G. Ab initio quasiharmonic equations of state for dynamically stabilized soft-mode materials. *Physical Review B* **65**, 184104 (2002).

[16] McWilliams, R. S. *et al.* Phase transformations and metallization of magnesium oxide at high pressure and temperature. *Science* **338**, 1330 (2012).

[17] Duffy, T. S. & Ahrens, T. J. Thermal expansion of mantle and core materials at very high pressures. *Geophysical Research Letters* **20**, 1103–1106 (1993).

[18] Karki, B., Wentzcovitch, R., de Gironcoli, S. & Baroni, S. High-pressure lattice dynamics and thermoelasticity of MgO. *Physical Review B* **61**, 8793–8800 (2000).

[19] Speziale, S., Zha, C.-S., Duffy, T. S., Hemely, R. J. & Mao, H.-k. Quasi-hydrostatic compression of magnesium oxide to 52 GPa: Implications for the pressure-volume-temperature equation of state. *Journal of Geophysical Research* **106**, 515 (2001).

[20] Svendsen, B. & Ahrens, T. J. Shock-induced temperature of MgO. *Geophysical Journal of the Royal Astronomical Society* **91**, 667–691 (1987).

[21] Alfè, D. *et al.* Quantum Monte Carlo calculations of the structural properties and the B1-B2 phase transition of MgO. *Physical Review B* **72**, 014114 (2005).

[22] Birch, F. Finite elastic strain of cubic crystals. *Physical Review* **71**, 809–824 (1947).

[23] Vinet, P., Ferrante, J., Rose, J. H. & Smith, J. R. Compressibility of solids. *Journal of Geophysical Research* **92**, 9319 (1987).

[24] Jackson, I. & Nielser, H. The elasticity of periclase to 3 GPa and some geophysical implication. In Akimoto, S. & Manghnani M. H. (eds.) *High-Pressure Research in Geophysics*, 93–133 (Center for Academic Publications, Tokyo, 1982).